Structure, Volume *21*

Supplemental Information

Molecular Organization and ATP-Induced Conformational Changes of ABCA4, the Photoreceptor-Specific ABC Transporter

Yaroslav Tsybovsky, Tivadar Orban, Robert S. Molday, Derek Taylor, and Krzysztof Palczewski

Inventory of Supplemental Information

This Supplemental Information contains Figure S1, Figure S2, Figure S3, Figure S4, Movie S1 and Table S1.

Figure S1 illustrates purification and biochemical properties of ABCA4 and provides details of the reference-based reconstruction and refinement used to obtain the structure of ABCA4 presented in Figure 1.

Figure S2 clarifies the location of the transmembrane region of ABCA4 proposed in Figure 2.

Figure S3 and associated text provide validation of differences between ligand-free and AMPPNP-bound structures of ABCA4 depicted in Figure 3.

Figure S4, related to Figure 4, illustrates the expected position of ABCA4 in the rim of a rod disc.

Movie S1 supplements Figure 3 by showing structural transitions in ABCA4 upon binding of AMPPNP.

Table S1 contains a list of peptides quantified for differences in H/D exchange in response to binding of AMPPNP; these differences are analyzed in Figure 3.

Supplemental Data

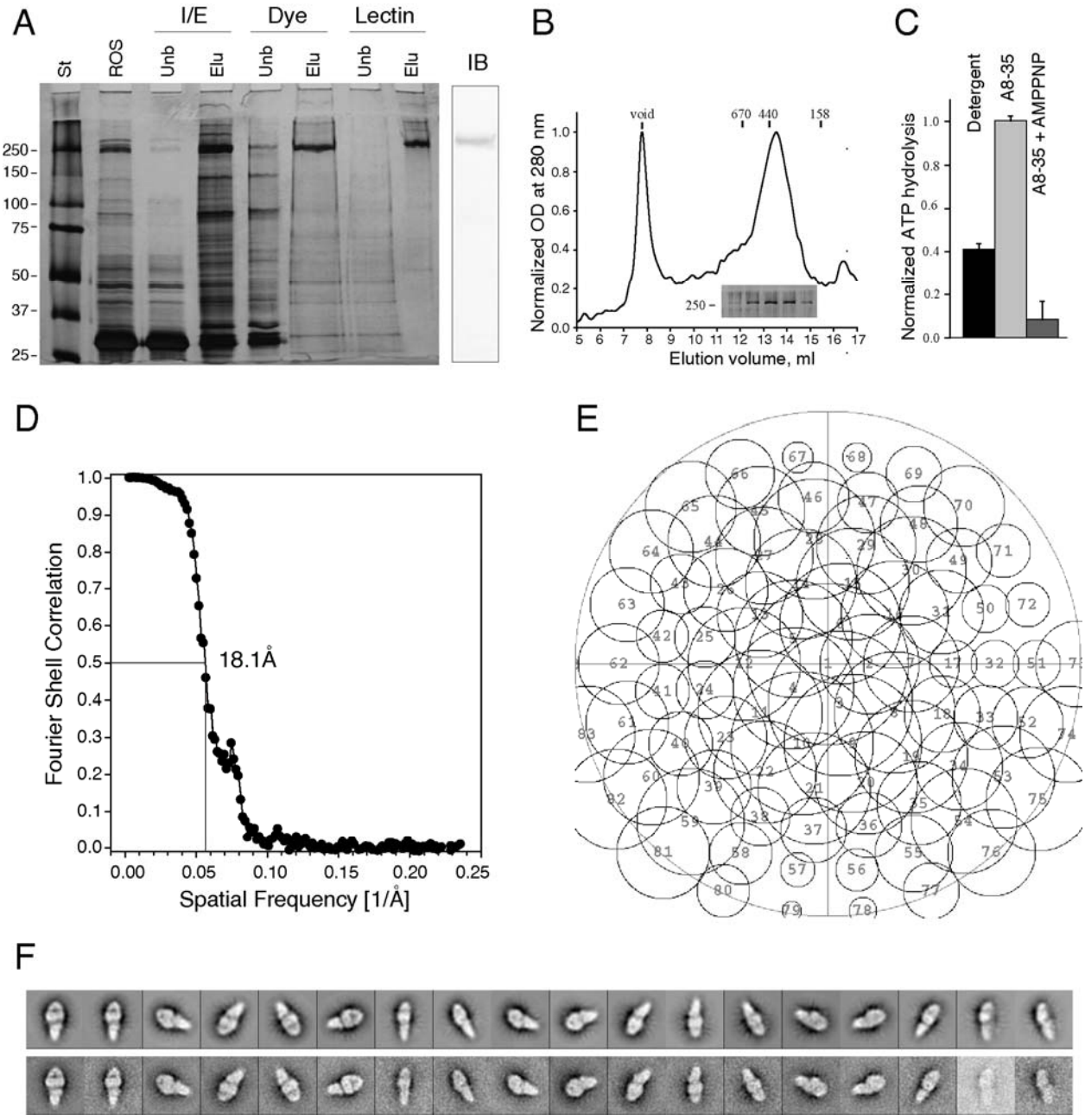

Figure S1, related to Figure 1. Purification, biochemical properties and reference-based projection alignment reconstruction of ABCA4. (*A*) A silver-stained SDS-PAGE gel (*left*) illustrating the isolation of ABCA4. Numbers indicate positions of molecular size markers in kDa. Purification steps are marked with *I/E* for ion exchange chromatography, *Dye* for ligand affinity

chromatography and *Lectin* for lectin affinity chromatography. *ROS*: detergent-solubilized ROS membranes; *Unb*: unbound fraction; *Elu*: eluted fraction. An immunoblot (IB) of purified ABCA4 is shown to the *right*. (*B*) Size exclusion chromatography of purified ABCA4 stabilized with Amphipol. Numbers (in kDa) above the chromatogram indicate the positions of calibration peaks. An SDS-PAGE gel separation of peak fractions is shown below the major curve. (*C*) Comparison of the ATPase activity of purified ABCA4 in detergent micelles *versus* Amphipol (*A8-35*). The far right bar reflects the ATPase activity of the Amphipol-embedded protein inhibited by addition of 1 mM of a non-hydrolysable ATP analog, AMPPNP. Data are represented as mean +/- SD. (*D*) Fourier shell correlation curve for the last refinement round suggesting a resolution of 18.1 Å based on the 0.5 threshold. (*E*) Distribution of 25,188 collected particles among 83 reference projections (15° angular sampling). The radii of the circles are proportional to the number of particles in each group. (*F*) Examples of the final model forward projections (*top*) and corresponding 2D average views (*bottom*) for a single defocus group containing 6,956 particles.

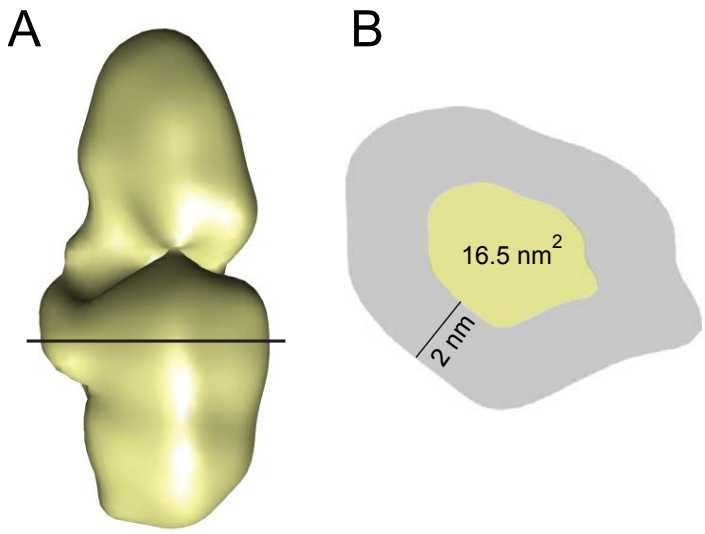

Figure S2, related to Figure 2. Estimation of the sectional area occupied by the twelve transmembrane helices of ABCA4. (*A*) The cross-section was taken perpendicularly to the vertical axis in the center of the proposed transmembrane region (*black line*). (*B*) A two nm-thick outer Amphipol A8-35 surfactant belt (gray) was subtracted from the cross-section. The remaining area (*yellow*) was assumed to be occupied by the transmembrane region.

Validation of differences observed in the ABCA4-AMPPNP complex *versus* ligand-free ABCA4 by using different initial 3D references.

The significance of the observed changes was validated in two ways (Figure S3). First, a second 3D map of the ABCA4-AMPPNP complex was independently determined using the RCT model as the initial reference. Because of the low resolution of the RCT model and the lack of strong structural features (Figure 1C, S3A), this allowed testing the reconstruction procedure for reproducibility and for the potential effect of reference bias. The resulting 18.8 Å-resolution structure showed the same conformational changes, including a constricted internal cavity and an altered shape of the 'head' region of AMPPNP-bound ABCA4 (Figure S3A). As before, the intradiscal region manifested no structural changes. Second, the ligand-free ABCA4 structure was reconstructed and refined using the ABCA4-AMPPNP complex as the starting model for reference-based alignment (Figure S3B). As expected, this resulted in a dilation of the internal cavity in the 'head' region of ABCA4, consistent with conformational changes induced strictly due to AMPPNP binding. Structural alterations between the ligand-free and AMPPNP-bound models are also reflected in the difference map (Figure S3C).

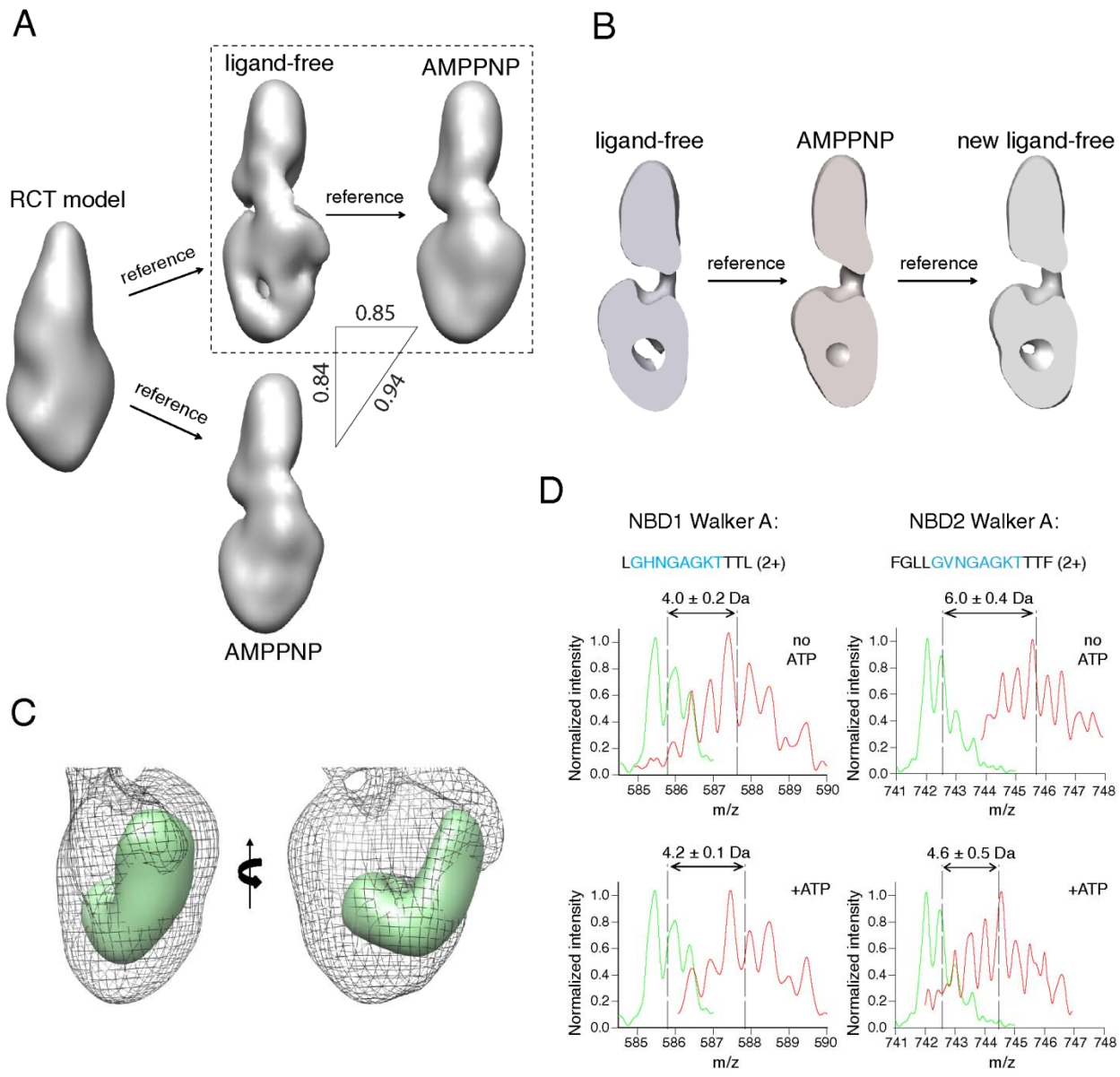

Figure S3, related to Figure 3. Differences observed in the ABCA4-AMPPNP complex *versus* ligand-free ABCA4 using single particle EM and H/D exchange. (*A*) ABCA4-AMPPNP complex structures (marked *AMPPNP*) obtained starting with the ligand-free or RCT model show the same differences from the ligand-free structure (constricted internal cavity and altered shape of the 'head' of the molecule). Numbers along the sides of the triangle indicate Pearson correlation coefficients between the corresponding maps. Structures used for biological interpretations are enclosed in a *black rectangle*. (*B*) When the ABCA4-AMPPNP structure is used as the initial reference for single particle analysis of ligand-free data, the features of the ligand-free structure (large internal cavity, altered 'head' shape) re-appear in the resulting model. (*C*) A difference map (*green*) calculated between the ABCA4-AMPPNP complex and ligand-free ABCA4

illustrates structural alterations in the 'head' region of the molecule. (*D*) Deuterium uptake during the ten minutes of incubation of ABCA4 with D_2O (see Supplemental Experimental Procedures) in the peptides that carry Walker A motifs of NBD1 (*left*) and NBD2 (*right*) is illustrated in the absence and presence of AMPPNP. The Walker A motifs located in the two corresponding doubly charged peptides, LGHNGAGKTTTL and FGLLGVNGAGKTTTF, are colored *light blue* within the peptide sequences. Peaks representing the non-deuterated doubly charged peptides are depicted in *green*, whereas peaks representing the same peptides after the intact protein has been incubated in deuterium prior to pepsin digestion are shown in *red*. Replacement of hydrogen in the main chain amide groups with heavier deuterium induced a positive shift in the peptide mass, which is proportional to the amount of incorporated deuterium. Mass differences between the non-deuterated and deuterated ions (Da) were evaluated using peak centroids (*dashed* lines) calculated with HX-Express (Weis et al., 2006). Average values of at least three independent experiments are shown along with standard deviations. The P values are 0.153 (no difference) for NBD1 and $p=5.5\cdot10^{-7}$ for NBD2.

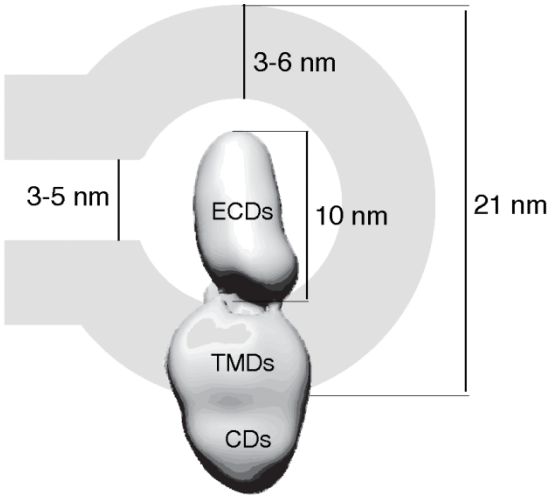

Figure S4, related to Figure 4. A model of ABCA4 positioning in the membrane of the rim of a rod disk, drawn to scale. *ECDs*, exocytoplasmic (intradiscal) domains; *CDs* cytoplasmic domains; *TMDs*, transmembrane domains.

Table S1, related to Figure 3. ABCA4 peptides analyzed for AMPPNP-induced changes in H/D exchange

Peptide	m/z	z +	MW (observed)	MW	sequence number	ATP-related motif?	AMPPNP-induced H/D exchange differences?
Exocytoplasmic domain 1							
FKLFHVFPRL	435.63	3	1304.88	1303.77	251	no	no
FIHRPSVQDLL	1324.86	1	1324.86	1324.74	287	no	no
FIHRPSVQDLL	663.21	2	1325.41			no	no
IRDTLENPTVKAFWNRQLGEEGITAE	996.88	3	2988.63	2987.52	451	no	no
FWNRQLGEEGITAEAVLNFLY	825.73	3	2475.18	2470.24	463	no	no
FRYIWGGF	1046.62	1	1045.62	1045.53	601	no	no
Cytoplasmic domain 1							
LGHNGAGKTTTL	1169.63	1	1170.17	1169.63	962	Walker A	no
LGHNGAGKTTTL	390.95	3	1170.85			Walker A	no
LGHNGAGKTTTL	585.59	2	1170.18			Walker A	no
FERELPGLVPGVC	708.65	2	1416.29	1415.74	918	before Walker A	no
TGLLPPTSGTVL	1155.68	1	1155.68	1155.66	977	after Walker A	no
FHHLTVAE	477.72	2	954.43	953.48	1015	after Walker A	no
FAGGTQQKRENINL	788.67	2	1576.33	1575.82	1286	no	no
IVQHVQAL	907.66	1	907.66	907.54	1349	no	no
NSGARL	617.53	1	617.53	617.34	1343	no	no
Exocytoplasmic domain 2							
LVKTYPAL	904.62	1	904.62	904.55	1532	no	no
IRSSLKSKF	356.02	3	1066.05	1065.64	1540	no	no
Cytoplasmic domain 2							
RPGECF	708.62	1	708.62	708.31	1961	before Walker A	no
KMLTGDTAVTSGDATVAGKSIL	1068.68	2	2136.35	2136.12	1981	after Walker A	no
FGLLGVNGAGKTTTF	1482.79	1	1482.79	1482.8	1966	Walker A	30% reduction
FGLLGVNGAGKTTTF	742.36	2	1483.72			Walker A	30% reduction
KDSLLI	343.73	2	686.45	688.42	2251	no	no

Supplemental Experimental Procedures

Materials. Frozen bovine retinas were purchased from W. L. Lawson Co. (Lincoln, NE). Mimetic Red3 ligand affinity resin was obtained from ProMetic Biosciences (Rockville, MD). GNL agarose and succinylated ConA were purchased from Vector Laboratories (Burlingame, CA). Amphipol A8-35 surfactant was provided by Affymetrix (Santa Clara, CA). Quantifoil holey carbon supported copper grids (2/1, 400 mesh) were from Quantifoil Micro Tools GmbH (Jena, Germany). The Luna 20 × 2.00 mm C18 column was purchased from Phenomenex (Torrance, CA).

Purification of ABCA4 from bovine rod outer segments. Bovine ROS membranes were isolated as described earlier (Tsybovsky et al., 2011) and solubilized at 4 °C with buffer containing 20 mM Bis-tris propane (BTP), pH 7.5, 10% glycerol, 35 mM NaCl, 1 mM DTT, 25 mM DDM and 0.2 mg/ml porcine brain polar lipids. ABCA4 was purified at 4 °C in four steps, all accomplished in one day. The first two steps were carried out under dim red light. All buffers prior to the size exclusion chromatography step contained 0.1 mg/ml porcine brain polar lipids. Solubilized membranes were first applied to a DE52 cellulose anion exchange column equilibrated with 20 mM BTP, pH 7.5, 10% glycerol, 35 mM NaCl, 1 mM DTT and 0.5 mM DDM (buffer A). The column was washed with the same buffer and bound proteins were eluted with 20 mM BTP, pH 7.5, 10% glycerol, 150 mM NaCl, 1 mM DTT and 2 mM DDM. The sample was then applied to a Mimetic Red3 ligand affinity column equilibrated with 20 mM BTP, pH 7.5, 10% glycerol, 100 mM NaCl, 1 mM DTT and 0.5 mM DDM (buffer B). After washing with buffer B, bound proteins were eluted with the same buffer containing 850 mM NaCl. Then 0.5 mM $CaCl_2$ and 0.5 mM $MnCl_2$ were added and the sample was applied to a GNL lectin affinity column equilibrated with 20 mM BTP, pH 7.5, 10% glycerol, 50 mM NaCl, 1 mM DTT, 0.5 mM DDM, 0.5 mM $CaCl_2$ and 0.5 mM $MnCl_2$ (buffer C). After washing with buffer C, ABCA4 was eluted with buffer containing 20 mM BTP, pH 7.5, 10% glycerol, 50 mM NaCl, 1 mM DTT, 1 mM DDM and 500 mM methyl α-D-mannopyranoside. To chelate remaining Ca^{2+} and Mn^{2+} ions, 1 mM EDTA was added. This was followed by incubation with 0.2 mg/ml Amphipol A8-35 for 30 min on ice. The sample then was concentrated in a 100 kDa cutoff centrifugal filter unit and subjected to size exclusion chromatography on a Superose 6 column equilibrated with 20 mM BTP, pH 7.5, 10% glycerol, 150 mM NaCl, 1 mM DTT (buffer D) in the absence of surfactants. For structural

studies of the ABCA4-AMPPNP complex, purified ABCA4 was incubated with 2 mM $MgCl_2$ and 1 mM AMPPNP at 4°C overnight.

ATPase activity measurements. To compare ATPase activity of ABCA4 in detergent micelles *versus* embedded in Amphipol A8-35, ROS membranes from 2 bovine retinas were solubilized in buffer containing 20 mM BTP, pH 7.5, 10% glycerol, 150 mM NaCl, 1 mM DTT and 18 mM 3-[(3-holamidopropyl)dimethylammonio]-1-propanesulfonate (CHAPS) and incubated with Rim3F4 mouse monoclonal antibody conjugated to agarose as described previously (Tsybovsky et al., 2011). After washing with the same buffer, ABCA4 was eluted using 20 mM BTP, pH 7.5, 10% glycerol, 150 mM NaCl, 1 mM DTT and 10 mM CHAPS (buffer E) supplemented with 1 mg/ml crude YDLPLHPRT peptide. The sample was divided in two equal parts and one was incubated for 30 min on ice with 0.2 mg/ml Amphipol A8-35 and then diluted 5x with buffer E containing no detergent to bring the CHAPS concentration to 2 mM (critical micelle concentration of CHAPS is 8 mM). The other half of the sample was diluted 5x with buffer E. $MgCl_2$ and (optionally) AMPPNP were added to final concentrations of 2mM and 1mM, respectively. The ATPase reaction was initiated by addition of 50 µl of ATP stock (0.5 mM ATP and 1 µCi [γ^{32}P]-ATP) to 500 µL of protein sample. Samples were incubated at 37 °C for 1 h and 100 µl aliquots were added to 1 mL of 10% activated charcoal in 10 mM HCl, vortexed and centrifuged. ^{32}P radioactivity in the resulting supernatants was counted in a LS 6500 multi-purpose scintillation counter (Beckman Coulter). Experiments were done in triplicates or quadruplicates.

Preparation of ABCA4-ConA complex. ROS membranes from 4 bovine retinas were solubilized in 2 ml of 20 mM BTP, pH 7.5, 10% glycerol, 150 mM NaCl and 0.1 mM DTT (buffer F) containing 25 mM DDM and incubated with 300 µL of Rim3F4 mouse monoclonal antibody conjugated to agarose for 3 h on ice in the dark. The resin was washed 8 times with 500 µL of buffer F with the DDM concentration reduced to 0.5 mM. The resin was then washed once with buffer F supplemented with 0.1 mg/ml Amhipol A8-35, followed by an incubation in the same buffer for 15 min. In the next step the resin was washed 8 times with 500 µL of buffer F in the absence of DDM and Amphipol A8-35 and then incubated for 30 min in the same buffer supplemented with 1 mM $CaCl_2$, 1 mM $MnCl_2$ and 0.5 mg/ml succinylated ConA. After 5 washes with buffer F containing 0.2 mM $CaCl_2$ and 0.2 mM $MnCl_2$, the ABCA4-ConA complex was eluted with buffer F supplemented with 1 mg/ml crude YDLPLHPRT peptide. Binding of ConA to ABCA4 was specific, as ConA alone did not bind to this resin. The complex was cross-linked with 1% glutaraldehyde for 15 min on ice. The cross-linking reaction was quenched with 0.2 M

Tris-HCl, pH 8.1, and the sample was immediately used to prepare EM grids as described below.

Transmission electron microscopy. Four µl samples of ABCA4 from peak size exclusion chromatography fractions were adsorbed for 2 min to glow-discharged, carbon film coated copper grids. Samples prepared for RCT reconstruction were supplemented with tobacco mosaic virus and adsorbed to glow-discharged, carbon coated Quantifoil holey carbon supported grids with 2 µm circular holes to simplify aligning untilted and tilted images. The grids were washed in two droplets of distilled water. For the ABCA4-AMPPNP complex, the water contained 0.2 mM $MgCl_2$ and 0.1 mM AMPPNP. After blotting, grids were stained with 1% (w/v) uranyl acetate. Data were collected with a FEI Tecnai F20 microscope (FEI, Eindhoven, Netherlands) operated at 200 kV and equipped with a Gatan US4000 UHS CCD camera (4K×4K) at magnifications of 40,500 (for RCT structure determination) and 70,400 (for all other datasets). For RCT, tilt pairs were collected at 0° and 45° angles. For reference-based three dimensional (3D) structure determination, 0° and 45° tilted micrographs were collected at a ratio of 1:1. For ABCA4-ConA complex analysis, all micrographs were collected at 0° tilt. Pixel sizes, at the specimen level, were 3.70 Å/pixel for the RCT micrographs and 2.13 Å/pixel for all other micrographs.

Structure determination by random conical tilt. The initial 3D model of apo ABCA4 was obtained by the RCT method (Radermacher et al., 1987) using the SPIDER software package (Frank et al., 1996). A total of 11,131 pairs of particles from untilted and 45° tilted micrographs were selected by using the RCT particle picking procedure implemented in JWeb (Frank et al., 1996) (Figure 3A). Particles were windowed into 110x110 boxes, normalized and centered. Two dimensional (2D) averages of untilted centered particles were calculated using the rotationally invariant K-means reference-free alignment and classification algorithm (Penczek et al., 1996) (Figure 3B). Tilted images corresponding to each 2D class were grouped, rotationally aligned and used to create 3D maps, which were subjected to translational refinement. Selected 3D maps were aligned and merged together. The merged 3D reconstruction was then subjected to iterative rounds of translational 3D refinement. Particles showing persistent excessive shifts were excluded, followed by a final round of translational 3D refinement. The final resolution of the RCT model (Figure 3C) was 38 Å.

Single-particle reconstruction using reference-based projection alignment. The 3D structure of ligand-free ABCA4 was determined by the referenced-based projection alignment method with the RCT model used as the initial reference. With the exception of particle picking,

reconstructions were done with SPIDER following a published procedure (Shaikh et al., 2008) with some modifications. For correct determination of defocus values and contrast transfer function (CTF) correction of tilted images, each micrograph was divided into 8 slices along the X axis perpendicular to the tilt axis of the microscope, and these slices were then treated as separate micrographs. The average defocus difference between adjacent slices was 0.11 µm. The defocus range was 0.2 to 1.2 µm underfocus. 25,188 particles were picked manually by using e2boxer from the EMAN2 software package (Tang et al., 2007) and introduced into the SPIDER reference-based projection alignment procedure (Shaikh et al., 2008) prior to the alignment step. The reconstructed structure was subjected to CTF-correction and multiple rounds of angular refinement. The isosurface level was chosen so that the 3D volume views corresponded well to 2D averages (Figure S1) and, at the same time, noise features were excluded from the map. Model volumes were consistent with values anticipated based on known specific volumes of protein and Amphipol.

The 3D structure of the ABCA4-AMPPNP complex was determined from a dataset of 38,090 particles by following the same protocol, with the final ligand-free ABCA4 or the RCT models used as initial references. The defocus range was 0.2 to 1.5 µm underfocus. The isosurface level of this map was chosen so that the volume of the model was identical to the volume of the ligand-free structure.

EM analysis of the ABCA4-ConA complex. Particles were picked manually by using e2boxer from the EMAN2 software package (Tang et al., 2007). Reference-free 2D class averages were calculated with SPIDER and EMAN2 software. Initial 3D models were obtained with the e2initialmodel module of EMAN2. Models displaying the characteristic ABCA4 shape with additional structural features consistent with the size and shape of the ConA dimer were selected and used as references for the reference-based projection alignment and 3D reconstruction procedure implemented in SPIDER (Shaikh et al., 2008).

Amide H/D exchange. H/D exchange experiments were conducted as previously described (Orban et al., 2012). Briefly, ten µl of pure ABCA4 (2.0 - 3.0 mg/ml) in buffer D was diluted with 70 µl of buffer containing 20 mM BTP, pH 7.5, and 10% glycerol prepared in D_2O. This buffer was supplemented with 2 mM $MgCl_2$ and 1 mM AMPPNP in experiments with the ABCA4-AMPPNP complex. The H/D exchange reaction was allowed to proceed for 10 min on ice and then was quenched by the addition of 10 µl ice-cold 1% formic acid which reduced the pH to 2.5. Ten µl of 8 mg/ml pepsin in water was immediately added and the sample was kept on ice for 15 min. Next, the sample (100 µl) was loaded on a C18 column with a temperature-

controlled auto sampler (Hewlett-Packard) set to 4 °C. The following HPLC method was used to separate peptides: 0–4 min, 98% of solution A comprised of H_2O with 0.1% (v/v) formic acid and 2% of solution B comprised of acetonitrile with 0.1% (v/v) formic acid; 4–15 min, gradient from 98% to 2% of solution A. Separation was performed with an Agilent 1100 HPLC system (Agilent Technologies, Santa Clara, CA) at a flow rate of 0.2 ml/min with the column kept on ice. The eluent was injected into a Thermo Finnigan LXQ mass spectrometer (Thermo Scientific, Waltham, MA) equipped with an electrospray ionization source operated in the positive ion mode. Activation type was set to collision-induced dissociation, normalized collision energy to 35 kV, capillary temperature to 370 °C, source voltage to 5 kV, capillary voltage to 43 V, the tube lens to 105 V, and spectra were collected over a 300–2,000 m/z range. All experiments were performed in quadruplicate. Statistical significance was evaluated by the unpaired Student's t-Test with a two-tailed distribution. Deuterium incorporation was evaluated with HX-Express (Weis et al., 2006).

Other methods. Resolutions of the EM structures were determined by the Fourier shell correlation method with a cut-off of 0.5. EM models were visualized with UCSF Chimera (Pettersen et al., 2004). Models of NBDs of ABCA4 were created with I-TASSER (Roy et al., 2010) and visualized with Pymol.

Supplemental References

Frank, J., Radermacher, M., Penczek, P., Zhu, J., Li, Y., Ladjadj, M., and Leith, A. (1996). SPIDER and WEB: processing and visualization of images in 3D electron microscopy and related fields. J Struct Biol *116*, 190-199.

Orban, T., Jastrzebska, B., Gupta, S., Wang, B., Miyagi, M., Chance, M. R., and Palczewski, K. (2012). Conformational dynamics of activation for the pentameric complex of dimeric G protein-coupled receptor and heterotrimeric G protein. Structure *20*, 826-840.

Penczek, P. A., Zhu, J., and Frank, J. (1996). A common-lines based method for determining orientations for N > 3 particle projections simultaneously. Ultramicroscopy *63*, 205-218.

Pettersen, E. F., Goddard, T. D., Huang, C. C., Couch, G. S., Greenblatt, D. M., Meng, E. C., and Ferrin, T. E. (2004). UCSF Chimera--a visualization system for exploratory research and analysis. J Comput Chem *25*, 1605-1612.

Radermacher, M., Wagenknecht, T., Verschoor, A., and Frank, J. (1987). Three-dimensional reconstruction from a single-exposure, random conical tilt series applied to the 50S ribosomal subunit of Escherichia coli. J Microsc *146*, 113-136.

Roy, A., Kucukural, A., and Zhang, Y. (2010). I-TASSER: a unified platform for automated protein structure and function prediction. Nat Protoc *5*, 725-738.

Shaikh, T. R., Gao, H., Baxter, W. T., Asturias, F. J., Boisset, N., Leith, A., and Frank, J. (2008). SPIDER image processing for single-particle reconstruction of biological macromolecules from electron micrographs. Nat Protoc *3*, 1941-1974.

Tang, G., Peng, L., Baldwin, P. R., Mann, D. S., Jiang, W., Rees, I., and Ludtke, S. J. (2007). EMAN2: an extensible image processing suite for electron microscopy. J Struct Biol *157*, 38-46.
Tsybovsky, Y., Wang, B., Quazi, F., Molday, R. S., and Palczewski, K. (2011). Posttranslational modifications of the photoreceptor-specific ABC transporter ABCA4. Biochemistry *50*, 6855-6866.

Weis, D. D., Engen, J. R., and Kass, I. J. (2006). Semi-automated data processing of hydrogen exchange mass spectra using HX-Express. J Am Soc Mass Spectrom *17*, 1700-1703.